Carbon stars with increased oxygen and nitrogen abundances: hydrostatic dust-free model atmospheres

B. Aringer, P. Marigo, W. Nowotny, L. Girardi, M. Mečina, A. Nanni

Monthly Notices
of the
ROYAL ASTRONOMICAL SOCIETY

MNRAS **487,** 2133–2147 (2019)
Advance Access publication 2019 May 23

doi:10.1093/mnras/stz1429

Carbon stars with increased oxygen and nitrogen abundances: hydrostatic dust-free model atmospheres

B. Aringer,[1,2★] P. Marigo,[1] W. Nowotny,[2] L. Girardi,[3] M. Mečina[2] and A. Nanni[1,4]

[1]*Dipartimento di Fisica e Astronomia Galileo Galilei, Università di Padova, Vicolo dell'Osservatorio 3, I-35122 Padova, Italy*
[2]*Department of Astrophysics, University of Vienna, Türkenschanzstraße 17, A-1180 Wien, Austria*
[3]*Osservatorio Astronomico di Padova – INAF, Vicolo dell'Osservatorio 5, I-35122 Padova, Italy*
[4]*Aix Marseille Univ., CNRS, CNES, LAM, 38, rue Frédéric Joliot-Curie 13388 Marseille, France*

Accepted 2019 May 8. Received 2019 April 28; in original form 2019 March 13

ABSTRACT

We have computed a grid of hydrostatic spherical COMARCS models for C stars covering metallicities from [*Z*/H] = 0 to −2 and values of the carbon excess [C−O] from 6.41 to 9.15, plus some temperature sequences, where the amount of oxygen and nitrogen is increased relative to a scaled solar element mixture. Such abundance variations may appear during the late stages of stellar evolution. Our study covers changes of [O/*Z*] and [N/*Z*] going up to +0.5. Based on the atmospheric structures we have calculated synthetic spectra and photometry for all of the models in a consistent way. The sequences with changed [O/*Z*] and [N/*Z*] can be used to derive correction terms, which are applied to the colours predicted for a certain combination of effective temperature, surface gravity, metallicity, and carbon excess. If one neglects these shifts in case of a variable oxygen amount, taking [C−O] instead of C/O gives much better results, since the first quantity dominates the formation of many important molecular species. For the warmer C giants with weaker pulsation it is in principle possible to determine [C−O], [O/*Z*], or [N/*Z*] from high-resolution spectra, when the opacities in the radiative transfer calculations for the models and observable properties are treated consistently. The corresponding changes due to the abundances often become significantly larger than the deviations caused by uncertainties of the stellar parameters or by an optically thin dust shell. Photometric data and low- or medium-resolution spectra are not sufficient to derive the mentioned quantities.

Key words: molecular data – stars: AGB and post-AGB – stars: atmospheres – stars: evolution – Hertzsprung–Russell and colour–magnitude diagrams – stars: late-type.

1 INTRODUCTION

After the exhaustion of helium in the core, low- and intermediate-mass stars with initial masses in the approximate range 0.8 $M_\odot \lesssim M_i \lesssim 7\ M_\odot$ may experience several mixing episodes during the latest stage of their evolution, which is called the thermally pulsing asymptotic giant branch (TP-AGB; Herwig 2005) phase. These events, known as the 'third dredge-up', take place in conjunction with the thermal pulses of the He-burning shell and enrich the convective envelope with newly synthesized elements, in particular ^{4}He, ^{12}C, ^{22}Ne, ^{25}Mg, and heavy isotopes produced by the *s*-process (Karakas & Lattanzio 2014). It is universally acknowledged that the corresponding surface enhancement explains the existence of intrinsic carbon stars characterized by a photospheric C/O ratio larger than one.

In this work we study the effect of enhanced oxygen and nitrogen abundances on the atmospheres and spectra of carbon stars. Concerning the second of the two elements, stellar evolution models predict that some enrichment of ^{14}N takes place as a result of the first dredge-up, which is a mixing episode happening when an object expands and moves towards its Hayashi line after the end of its time on the main sequence (e.g. Forestini & Charbonnel 1997). The amount of additional ^{14}N is expected to depend on mass and metallicity. For instance, following recent PARSEC (Bressan et al. 2012) calculations for stars with a solar-like starting composition (metal mass fraction $X_Z = 0.014$), it has been found that after the first dredge-up the surface nitrogen increases with the initial mass from [N/*Z*] ≃ 0.2 at $M_i = 1.0\ M_\odot$ to [N/*Z*] ≃ 0.55 at $M_i = 3.4\ M_\odot$. A further enrichment may appear in intermediate-mass objects with $M_i > 3.5 - 4.0\ M_\odot$ caused by the occurrence of the second dredge-up at the base of the early AGB, when the H-burning shell is temporarily extinguished. For $X_Z = 0.014$ the [N/*Z*] value in these giants can grow up to ≃0.65 at $M_i = 6.0\ M_\odot$. In stars with lower

★ E-mail: bernhard.aringer@unipd.it

metallicity the PARSEC models predict that the increase of nitrogen relative to its initial abundance becomes a bit larger. For example, at $X_Z = 0.001$ [N/Z] is typically higher by ≈0.05.

In current standard stellar evolution calculations usually no increase of the oxygen abundance is predicted as a consequence of the first, second, and third dredge-up episodes. However, a possible enrichment of ^{16}O may be expected during the TP-AGB phase under particular conditions. Allowing for overshoot beyond the Schwarzschild border of the pulse-driven convective zone during the third dredge-up, some amount of primary ^{16}O produced by the reaction ^{12}C(α, γ)^{16}O can be mixed up to the surface (Herwig 2000). This scenario seems to be supported by abundance analyses of PG1159 stars (e.g. Werner & Herwig 2006), post-AGB objects (e.g. De Smedt et al. 2016), and planetary nebulae (e.g. García-Hernández et al. 2016).

Following earlier work by Jørgensen, Hron & Loidl (2000) and Loidl, Lançon & Jørgensen (2001), Aringer et al. (2009) have published a grid of 746 hydrostatic COMARCS models for carbon star atmospheres, which covers effective temperatures between 2400 and 4000 K with C/O ratios ranging from 1.05 to 5.0. The included metallicities are [Z/H] = 0, −0.5, and −1 (see the definition in Section 2.1). The calculations, where spherical symmetry and local thermodynamic plus chemical equilibrium have been assumed, did not take the formation of dust into account. Based on the models the authors computed synthetic spectra and photometry, which could then be compared to observations. One of the main conclusions from this work is that down to about 2800 K the COMARCS atmospheres are able to predict the measured colours of carbon stars, while for cooler objects the simulated results appear much too blue. Those large deviations occur because of circumstellar dust shells and the effects of pulsation plus mass-loss on the radial temperature–pressure structures.

Compared to the work of Aringer et al. (2009) the new COMARCS models used here have been calculated with updated molecular opacities applied already in Aringer et al. (2016), where K and M stars are studied. Some information concerning these changes can be found in the next section. The impact on the photometric results is discussed in Section 4. Our new COMARCS grid covers also a much larger set of abundance combinations, including a very low metallicity of [Z/H] = −2, C/O ratios from 1.01 to 10 and more, as well as mixtures with an enrichment of oxygen and nitrogen. Gonneau et al. (2017) compared medium- to high-resolution spectra of carbon stars taken with the X-shooter instrument to synthetic ones based on the current models. They arrive at a conclusion similar to the results of Aringer et al. (2009). While the hydrostatic calculations describe the warmer objects with weak pulsations quite well, the cooler sources are dominated by dust and dynamic effects on the structures.[1]

Following the investigations of Nowotny et al. (2011, 2013), a grid of dynamic models for cool carbon giants with solar metallicity has been produced by Eriksson et al. (2014), who has also published a data base containing spectra and photometric properties as a function of time. These calculations consider pulsations plus the formation and opacity of dust, which may drive intense stellar winds. Thus, they can explain the very red colours connected to high mass-loss rates. The models were computed with a version of the DARWIN code described in Höfner et al. (2016). A set-up similar to the one for the COMARCS atmospheres has been used to determine the observable properties. The authors show that their approach reproduces the measured colours and outflow velocities of cool pulsating carbon stars quite well. The main problem of those models is the limited capability to describe objects with weak mass-loss and reddening, which are very common. DARWIN calculations also covering lower metallicities have recently been published by Bladh et al. (2019).

Since the circumstellar reddening causes in pulsating carbon stars having mass-loss by far the strongest effect on the overall spectral energy distribution, it is a very common approach to determine the colours by combining a central hydrostatic atmosphere with an extra description of the dust shell. Compared to the dynamic calculations this procedure takes much less time, which is an advantage if big grids are needed. In addition, the large number of objects generating a weak wind can be reproduced without any problems. On the other hand, such models do not consider temporal variations resulting in complicated structures, and using them introduces free parameters. For example, the mass-loss rate or something equivalent to it has to be assumed in all cases. One approach is the computation of stationary winds including dust formation and opacity like in Dell'Agli et al. (2015) or Nanni et al. (2016). Shell models based completely on parameters except for the radiative transfer were used, for instance, by Srinivasan, Sargent & Meixner (2011), Groenewegen (2012), Gullieuszik et al. (2012), and Riebel et al. (2012). The method of applying circumstellar reddening to a central hydrostatic atmosphere is also the standard tool for the determination of colours of cool giants in connection with population synthesis codes (Marigo et al. 2008, 2017; Pastorelli et al. 2019).

2 MODEL ATMOSPHERES AND SYNTHETIC SPECTRA

In order to simulate the atmospheric structures of carbon stars we use the newest hydrostatic models from the COMARCS grid described in Aringer et al. (2016), where one can find more details concerning the calculations and the included opacity sources. The corresponding data base, which contains mainly objects of spectral type K, M, S, and C, was significantly extended in the domain with C/O > 1 for the purpose of the investigation presented here. An updated list of the available stellar parameter and elemental abundance combinations is given in http://stev.oapd.inaf.it/atm. Concerning the atomic and molecular transitions taken into account and the treatment of convection, all models used in this work have the same set-up as in Aringer et al. (2016). The COMARCS program, where spherical symmetry and local thermodynamic and chemical equilibrium are assumed, was originally developed based on a version of the MARCS code (Gustafsson et al. 1975, 2008) described in Jørgensen, Johnson & Nordlund (1992) and Aringer, Jørgensen & Langhoff (1997). The formation of dust is not included.

Compared to the previous COMARCS grid of carbon stars published by Aringer et al. (2009), some molecular opacities have been added and updated as described in Aringer et al. (2016). For example, the CrH bands are much weaker in the new calculations. As a consequence, their effect on medium- or low-resolution spectra and photometry became almost negligible. We also want to note that the scaling of the C_2 list from Querci, Querci & Tsuji (1974) at wavelengths above 1.15 μm, which has been suggested by Loidl et al. (2001) and used as a standard for the 2009 models, is not applied anymore. It was already found by Aringer et al. (2009) that it causes synthetic $(H - K)$ colours shifted by 0.1 mag with respect to

[1]Many of the carbon star models used here were already included in the original data base connected to Aringer et al. (2016). However, we did not discuss them in that paper.

the observations. At least for the bluer objects with weak pulsations and low mass-loss rates these systematic deviations disappear, if the original data are not modified. Some of the photometric changes between the old and the current carbon star grid will be discussed later in this work.

When calculating observable properties of our models, we have again followed the approach described in Aringer et al. (2016). Synthetic medium-resolution $R = 10\,000$ opacity sampling (OS) and convolved low-resolution $R = 200$ spectra were produced with the COMA code (Aringer 2000), which was already used to create gas absorption data for the generation of the COMARCS atmospheres. Based on the output of these computations, we could determine photometric results for a large number of filters covering many different systems. Tables with the corresponding bolometric corrections (BCs) are available at http://stev.oapd.inaf.it/atm. This data base, which comprises the complete COMARCS grid, including all models used here, also contains the low- and medium-resolution spectra. It will be extended if further results are produced. We want to note that due to their statistical nature the OS spectra should never be directly compared to observations.

Concerning the photometric data we want to note that in this work only visual and near-infrared magnitudes, which were determined according to the definition from Bessell (1990) and Bessell & Brett (1988), will be discussed. The *V*, *J*, *H*, and *K* values and corresponding colours appearing in Sections 3.4 and 4 are based on this system (Bessell).

In addition to the standard approach, we have used COMA to calculate high-resolution spectra with $R = 300\,000$ covering the wavelength range between 1.7046 and 1.7064 μm. This was done only for a few selected models having effective temperatures of 2800 and 3300 K. Some of the results are shown in Fig. 4.

2.1 Model parameters

Temperature sequences of COMARCS carbon star models calculated with oxygen and nitrogen abundances deviating from the standard set-up of a scaled solar composition, which is described in Section 2.1.1, are only available for $\log(g\ [\mathrm{cm\,s^{-2}}]) = 0.0$ and the mass of the Sun. Thus, the investigation presented here remains restricted to this selection of the corresponding two parameters. The effect of varying their values has been discussed in detail by Aringer et al. (2009). As was already mentioned before, some of the opacities were revised since then, resulting in moderate differences concerning spectra and colours. However, the relative changes due to the stellar properties remain almost the same. Because the production of complete carbon star subgrids containing many combinations of values for the effective temperature, surface gravity, and mass takes much time, they exist in the COMARCS data base only for standard cases with scaled solar abundances (at the moment all sets with [*Z*/H] = 0 and some with −0.5). Their upper limit of $\log(g\ [\mathrm{cm\,s^{-2}}])$ is usually 2.0, while the lower one ranges between 0.0 for $T_{\rm eff} > 3400$ K and −1 for the coolest objects. In addition, masses from 1.0 to 3.0 $\mathrm{M}_{\odot}$ are covered. Detailed information concerning the available COMARCS models can be found at the Internet link mentioned above.

The $\log(g\ [\mathrm{cm\,s^{-2}}]) = 0.0$ sequences discussed here and the COMARCS carbon star subgrids usually cover the effective temperature range from 2500 to 4400 or 4000 K with a maximum step size of 100 K. For a few of the standard cases with scaled solar abundances the lower limit is 2600 K (C/O = 1.01 and 1.10 at [*Z*/H] = 0). Like in Aringer et al. (2009) the microturbulent velocity was set to $\xi = 2.5\,\mathrm{km\,s^{-1}}$. Concerning the chemical composition of the Sun, which represents the reference for all other mixtures used in this work, we followed the assumptions in Aringer et al. (2016) based on Caffau, Ludwig & Steffen (2009a) and Caffau et al. (2009b). The resulting C/O ratio is close to 0.55.

Table 1. The opacity sets used for this work. The overall metallicity [*Z*/H] and additional changes of the amount of oxygen [O/*Z*] or nitrogen [N/*Z*] are listed with respect to the solar values. The elemental abundances of O, C, and Fe correspond to number densities: $\log(\varepsilon_{\mathrm{Fe,O,C}}/\varepsilon_{\mathrm{H}}) + 12$. Combinations taken from the standard COMARCS grid are marked with an 's'.

[*Z*/H]	C/O	[C−O]	[O/*Z*]	[N/*Z*]	O	C	Fe
−2.0	1.40	6.41	0.00	0.0	6.80	6.95	5.56^{s}
−2.0	2.00	6.80	0.00	0.0	6.80	7.10	5.56^{s}
−2.0	6.00	7.50	0.00	0.0	6.80	7.58	5.56^{s}
−2.0	10.00	7.76	0.00	0.0	6.80	7.80	5.56^{s}
−2.0	29.47	8.26	0.00	0.0	6.80	8.27	5.56
−2.0	10.00	8.26	+0.50	0.0	7.30	8.30	5.56
−2.0	10.00	8.26	+0.50	+0.5	7.30	8.30	5.56
−1.0	1.40	7.36	−0.04	0.0	7.76	7.91	6.56
−1.0	1.58	7.53	−0.04	0.0	7.76	7.96	6.56
−1.0	2.00	7.76	−0.04	0.0	7.76	8.06	6.56
−1.0	2.04	7.78	−0.04	0.0	7.76	8.07	6.56
−1.0	2.95	8.05	−0.04	0.0	7.76	8.23	6.56
−1.0	3.90	8.22	−0.04	0.0	7.76	8.35	6.56
−1.0	1.10	6.80	0.00	0.0	7.80	7.84	6.56^{s}
−1.0	1.40	7.41	0.00	0.0	7.80	7.95	6.56^{s}
−1.0	2.00	7.80	0.00	0.0	7.80	8.10	6.56^{s}
−1.0	4.00	8.28	0.00	0.0	7.80	8.40	6.56^{s}
−1.0	8.00	8.65	0.00	0.0	7.80	8.71	6.56^{s}
−1.0	1.40	7.53	+0.12	0.0	7.92	8.07	6.56
−1.0	2.00	8.05	+0.25	0.0	8.05	8.35	6.56
−0.5	1.05	7.00	0.00	0.0	8.30	8.32	7.06^{s}
−0.5	1.10	7.30	0.00	0.0	8.30	8.34	7.06^{s}
−0.5	1.40	7.91	0.00	0.0	8.30	8.45	7.06^{s}
−0.5	2.00	8.30	0.00	0.0	8.30	8.60	7.06^{s}
−0.5	4.00	8.78	0.00	0.0	8.30	8.90	7.06^{s}
−0.5	8.00	9.15	0.00	0.0	8.30	9.21	7.06^{s}
0.0	1.01	6.81	0.00	0.0	8.80	8.81	7.56^{s}
0.0	1.05	7.50	0.00	0.0	8.80	8.82	7.56^{s}
0.0	1.10	7.80	0.00	0.0	8.80	8.84	7.56^{s}
0.0	1.32	8.30	0.00	0.0	8.80	8.92	7.56
0.0	1.40	8.41	0.00	0.0	8.80	8.95	7.56^{s}
0.0	2.00	8.80	0.00	0.0	8.80	9.10	7.56^{s}
0.0	1.10	8.30	+0.50	0.0	9.30	9.34	7.56
0.0	1.10	8.30	+0.50	+0.5	9.30	9.34	7.56

In Table 1 we list the various abundance sets available for carbon stars. The overall metallicity is described by the parameter [*Z*/H], which corresponds to the logarithm of the number density (ε) for the bulk of the individual elements heavier than He divided by the value for H (ε_{H}) and scaled relative to the solar ratio. Since we use here the common definition, where $\log(\varepsilon_{\mathrm{H}})$ is set constant to 12, and no COMARCS models with special deviations of the Fe content exist, the quantities [*Z*/H], [Fe/H], and $\log(Z/Z_{\odot})$ are always equal. A variation of the nitrogen abundance and oxygen abundance with respect to that of the other metals does not change them. The corresponding number densities are described in a similar way by the solar scaled logarithmic ratios [O/*Z*] and [N/*Z*]. The last parameter needed to characterize our sets is C/O ($\varepsilon_{\mathrm{C}}/\varepsilon_{\mathrm{O}}$), which has to be larger than 1 in order to form a carbon star. Table 1 contains also the individual abundances of O, C, and Fe defined by $\log(\varepsilon_{\mathrm{Fe,O,C}}/\varepsilon_{\mathrm{H}}) + 12$ (solar values: 8.80 for O, 8.54 for C, and 7.56 for Fe). In addition, we list the important quantity [C−O], which stands for the difference of the number densities of those two elements. It gives an estimate for

the amount of free carbon atoms not bound in CO and has to be calculated by $\log((\varepsilon_C - \varepsilon_O)/\varepsilon_H) + 12$.

2.1.1 *Standard models with scaled solar abundances*

In order to obtain the chemical standard mixtures for the COMARCS grid (marked with 's' in Table 1) we have first scaled the abundances of the elements heavier than He to the chosen overall metallicity [*Z*/H] as explained above. Subsequently, the amount of carbon was changed according to the selected C/O ratio. At the moment models with values of 1.01, 1.05, 1.10, 1.40, 2.0, 4.0, 6.0, 8.0, and 10.0 are available. The coverage depends on [*Z*/H], since we have to take into account that for metal-poor stars the increase of C/O following a dredge-up event is much larger. In these objects one needs also a higher ratio to get a certain amount of free carbon atoms [C−O].

Our data base includes also two $\log(g\ [\mathrm{cm\,s^{-2}}]) = 0.0$ sequences with scaled solar abundances, which have the same [C−O] values as the models discussed in the next section, where the amount of oxygen and nitrogen is increased. The corresponding parameters are C/O = 1.32, [C−O] = 8.30 at [*Z*/H] = 0.0 and C/O = 29.47, [C−O] = 8.26 at [*Z*/H] = −2.0.

2.1.2 *Models with a fixed enhancement of oxygen and nitrogen*

In order to study the effect of deviations from a scaled solar chemical mixture in carbon stars we have produced two classes of models, where only oxygen or oxygen and nitrogen are enhanced by a fixed factor. The corresponding values are [O/*Z*] = +0.5 and [O/*Z*] = [N/*Z*] = +0.5. This investigation was done for two abundance sets from the standard COMARCS grid keeping the overall metallicity and the C/O ratio constant. They have the following parameters: C/O = 1.10 at [*Z*/H] = 0.0 and C/O = 10.0 at [*Z*/H] = −2.0. It should be noted that an enhancement of oxygen will result in a larger amount of free carbon atoms if C/O and [*Z*/H] remain unchanged. However, as was already mentioned in the previous section, in both cases discussed here we have also computed sequences with scaled solar abundances and the same [C—O].

2.1.3 *Enhancement of oxygen based on stellar evolution models*

We replaced the carbon and oxygen abundances in our standard COMARCS sets having [*Z*/H] = −1 with the ones taken from a TP-AGB stellar evolution track, which was computed with the COLIBRI code (Marigo et al. 2013) adopting [Fe/H] = −1 and an initial mass of 2.0 $M_\odot$. In order to take the effect of an O enrichment into account, the following mass fractions of the involved isotopes have been assumed for the intershell: $X(^{12}C) = 0.48$ and $X(^{16}O) = 0.17$. These values are very close to the ones that match the observed photospheric composition of some PG1159 stars (see Herwig 2000 for a detailed discussion). The two stages, where the C/O ratio reaches 1.4 and 2.0 as a result of the third dredge-up episodes, have been selected to create sequences of synthetic atmospheres and spectra. This corresponds to [O/*Z*] values of +0.12 and +0.25, which are smaller than the fixed shifts discussed in the previous section.

We have also calculated COMARCS atmospheres using the initial oxygen abundance of the stellar evolution models taken from a phase before the start of the third dredge-up. It has a value that is quite close to the one in our standard grid. We do not expect that the corresponding shift of [O/*Z*] = −0.04 will cause any significant changes of the radial temperature and pressure structures or the spectra. For both of the sequences with an oxygen enhancement three classes of such COMARCS models were produced having the same C/O (1.4, 2.0), [C−O] (7.53, 8.05), and absolute carbon abundance (8.07, 8.35).

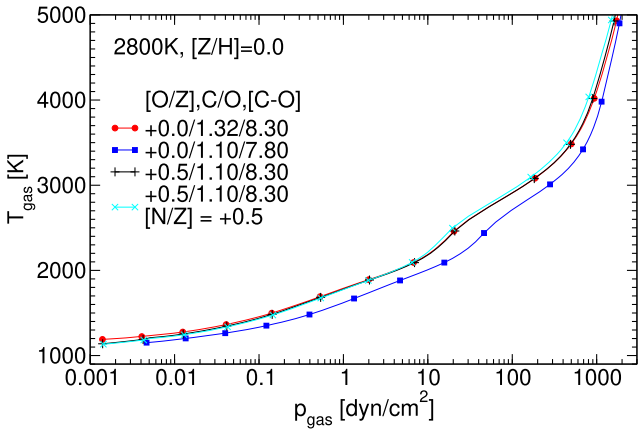

Figure 1. The effect of an increased oxygen and nitrogen abundance on the atmospheric temperature versus gas pressure structure is shown for different COMARCS models with $T_{\rm eff} = 2800$ K, $\log(g\ [\mathrm{cm\,s^{-2}}]) = 0.0$, and solar mass and metallicity. Results obtained adopting [O/*Z*] = +0.5 (black) and [O/*Z*] = +0.5, [N/*Z*] = +0.5 (cyan) are compared to calculations for the standard composition ([O/*Z*] = 0, [N/*Z*] = 0) with a constant C/O (blue) or [C−O] (red). The plot symbols placed along the curves mark steps of $\Delta\log(\tau_{\rm Ross}) = 0.5$ starting with −5 at the outer edge.

3 RESULTS

In this section we discuss some of the important results from our investigation concerning atmospheric structures, spectra with low or high resolution, and photometric colours.

3.1 Model structures

In Fig. 1 we show the temperature pressure structures of four COMARCS models with $T_{\rm eff} = 2800$ K and [*Z*/H] = 0.0. The results, where only oxygen or oxygen and nitrogen have been enhanced by [O/*Z*] = +0.5 and [N/*Z*] = +0.5, are compared to calculations with scaled solar abundances and the same C/O (1.10) or [C−O] (8.30). One can see that the atmospheres behave in a very similar way if the excess of free carbon atoms remains constant, while a decrease of this quantity causes significant changes. For the lower value of [C−O] the curve moves to cooler temperatures. Since the corresponding typical shift ranges from 100 to 300 K, it has a considerable effect on the emerging spectra. The main reason for this variation of the structure is that the amount of free carbon influences the formation of species like C_2, C_3, HCN, and C_2H_2, which are important for the overall opacity.

If the stars get much warmer than about 3000 to 3200 K, the role of [C−O] as a dominant parameter becomes less pronounced. This is due to the fact that the abundance and importance of the mentioned molecules decrease with a higher temperature. In the hotter models also variations of [O/*Z*] at a constant carbon excess and of [N/*Z*] can have a moderate effect on the structures.

3.2 Low-resolution spectra

In Figs 2 and 3 we present low-resolution spectra covering the range from 0.6 to 2.4 μm, which have been computed for the four

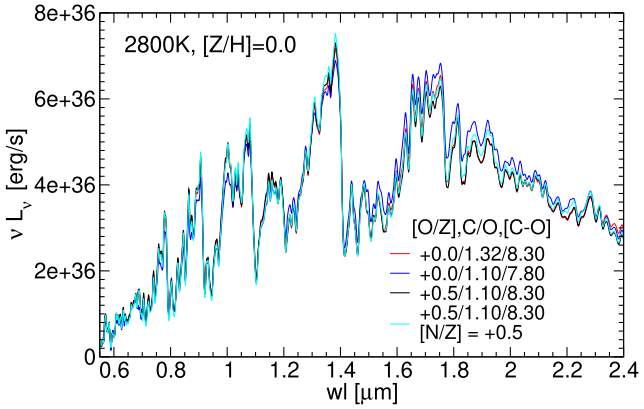

Figure 2. Low-resolution $R = 200$ spectra computed from COMARCS models with $T_{\rm eff} = 2800$ K, $\log(g\ [{\rm cm\,s^{-2}}]) = 0.0$, and solar mass and metallicity. The effect of an increased oxygen and nitrogen abundance is shown. Results obtained adopting $[O/Z] = +0.5$ (black) and $[O/Z] = +0.5$, $[N/Z] = +0.5$ (cyan) are compared to calculations for the standard composition ($[O/Z] = 0$, $[N/Z] = 0$) with a constant C/O (blue) or [C−O] (red).

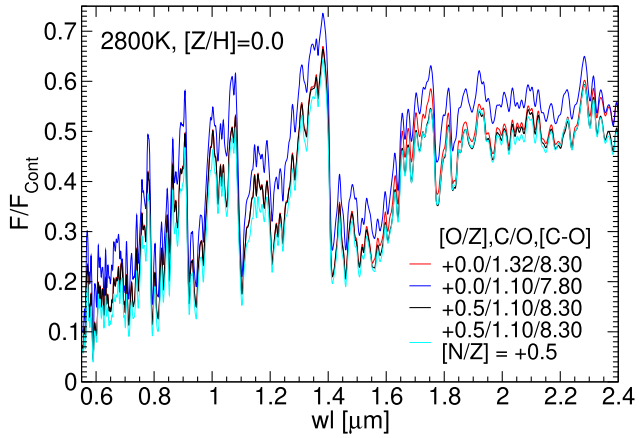

Figure 3. Continuum-normalized low-resolution $R = 200$ spectra based on COMARCS atmospheres. The included models and the corresponding line colours are the same as in Fig. 2.

COMARCS models with $T_{\rm eff} = 2800$ K and $[Z/H] = 0.0$ used already in Fig. 1. This allows us to study the effects of an enrichment of oxygen and oxygen plus nitrogen if the C/O or [C−O] value remains constant. The results shown in Fig. 3 are normalized with respect to a radiative transfer calculation, where all line opacities have been set to zero. Using this inconsistent approach, one can estimate the intensity of the atomic and molecular absorption produced in different regions of the stellar spectra without the influence of changes caused by the continuum.

Looking at Fig. 3 we can conclude that the COMARCS atmosphere with the lower [C−O] value (7.80) has in general clearly the weakest line absorption, while the strongest one is usually created by the model having an increased amount of oxygen and nitrogen. For the cool effective temperature of the selected examples and the shown spectral range the opacity is dominated by molecular transitions of CN, C_2, C_3, HCN, and C_2H_2. Atomic features do not play an important role. Thus, the mentioned behaviour agrees with the expectations, since a smaller amount of free carbon will decrease the formation of the species listed above. In addition, CN and HCN may become more abundant if a larger fraction of nitrogen is available. However, the relation could be less simple, because the opacity of the discussed molecules changes the atmospheric structure, which then influences again the chemical equilibrium. One should also take into account that in cool objects it is not possible to measure the absorption relative to an absolute continuum, since even at higher resolution all regions of the spectra are significantly affected by many overlapping lines. The observable depth of certain features with respect to their surrounding can often show a behaviour that does not reflect the variation of the total intensity of the corresponding molecular bands.

The unscaled spectra and deduced photometric data will be affected by millions of weak overlapping lines as well as by the level and shape of the continuum depending on the atmospheric structure. Despite the different intensity of their molecular absorption, especially when the [C−O] value is varied, all results shown in Fig. 2 look quite similar. The general agreement of the overall fluxes can be explained with the constant integrated luminosity of the consistent calculations. But also on the smaller scales we find in many regions only weak or no changes. This is at least partly due to a saturation of the strong lines and the large influence of the molecular opacities on the structures. Some moderate variations appear in the range around 1.8 μm, where a lower excess of free carbon atoms decreases the intensity of the features. However, in contrast to the normalized data a broader spectral interval with a clear positive correlation between the studied abundances and the depth of the bands does not exist.

For a warmer star with an effective temperature of 3300 K the behaviour is similar. In the normalized spectra the overall molecular absorption clearly grows with a higher carbon excess or nitrogen abundance. The variation of the unscaled results remains again much smaller. Never the less, the correlation of the depth with the [C−O] and [N/Z] values is for many of the features there more pronounced than at 2800 K.

3.3 High-resolution spectra

The different panels in Fig. 4 contain high-resolution spectra based on COMARCS models with an effective temperature of 2800 or 3300 K and a metallicity of $[Z/H] = 0$ or -1. The shown wavelength range between 1.7047 and 1.7064 μm is a typical example for a region characterized by a moderate molecular absorption. Like in Fig. 3 the data are normalized relative to a calculation where all line opacities have been omitted. Compared to the unscaled results this makes apart from the general flux level no difference, since the continuum does not change within such a narrow interval. However, the shown spectra of the cooler models demonstrate clearly that for the entire frequency range a large fraction of the radiation is blocked by many weak overlapping molecular transitions. Even at a high resolution there exists no point that is not affected by strong line absorption. This agrees with the results found in the previous section. The situation changes if the atmospheres become warmer. In Fig. 4 one can see that the spectra computed from the models having 3300 K already include some narrow regions where the flux is close to the continuum level.

For the solar metallicity Fig. 4 contains the abundance combinations already used in Figs 1−3. This shows the spectral variation with changed values of [O/Z] and [O/Z] plus [N/Z] if C/O or [C−O] is kept constant. In the case of $[Z/H] = -1$ we present results where the oxygen enrichment has been taken from the stellar evolution calculations. COMARCS models with $[O/Z] = 0.25$ and $C/O = 2.0$ are compared to similar ones having $[O/Z] = -0.04$ and the same C/O, [C−O] (8.05) or total amount of carbon (8.35). In addition, we include spectra for a much lower C/O ratio of 1.4.

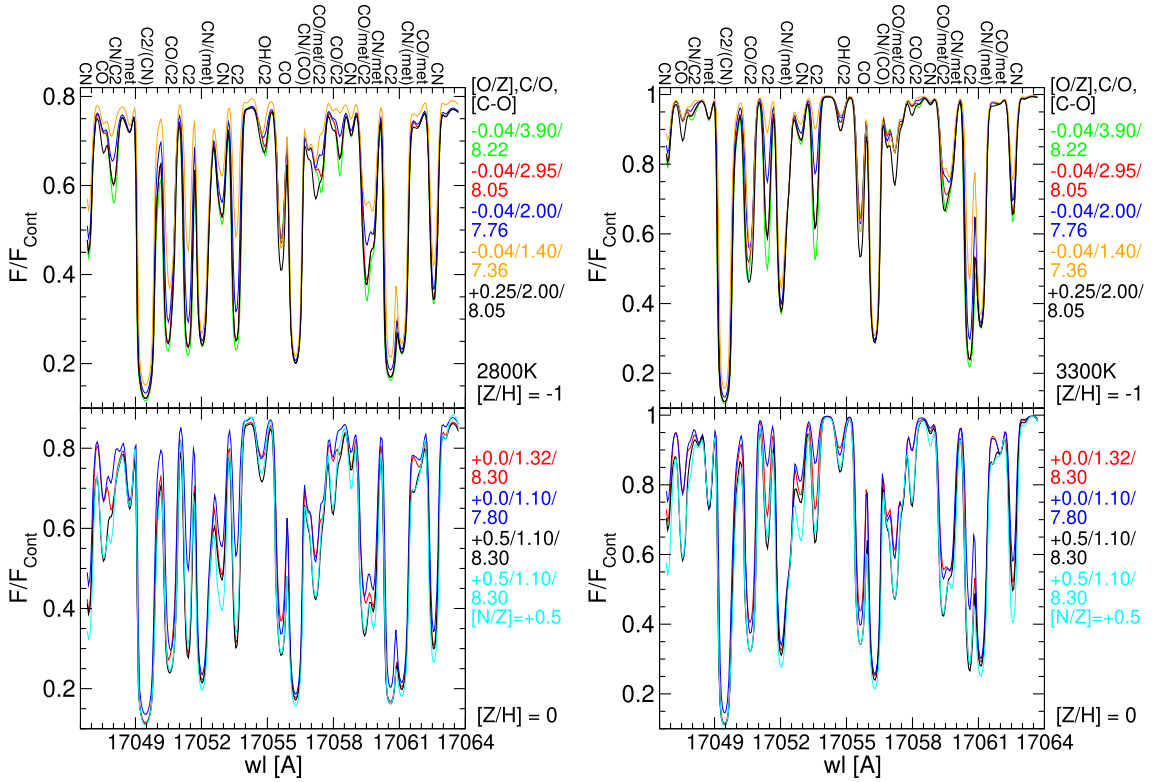

Figure 4. High-resolution $R = 300\,000$ spectra based on COMARCS models with $\log(g\ [\mathrm{cm\,s^{-2}}]) = 0.0$ and one solar mass having $T_{\rm eff} = 2800$ K (left-hand panels) or 3300 K (right-hand panels) and [*Z*/H] = 0 (lower panels) or −1 (upper panels). The data are normalized relative to a calculation without molecular and atomic line opacities. The different absorption features have been marked with the species creating them. 'met' stands for transitions due to metals. If a certain component of a blend is much weaker than the rest, it was put in brackets. For [Z/H] = −1 we compare an oxygen-enriched model ([O/Z] = 0.25, C/O = 2.0, [C−O] = 8.05, black) to calculations with [O/Z] = −0.04 having a constant C/O ([C−O] = 7.76, blue), [C−O] (C/O = 2.95, red), total amount of carbon $\varepsilon_{\rm C}$ (C/O = 3.90, [C−O] = 8.22, green), and a lower C/O of 1.4 ([C−O] = 7.36, orange). For [Z/H] = 0 the shown abundance combinations and the corresponding line colours are the same as in Fig. 2.

The intensities of the spectral features, which can be uniquely assigned to certain molecules, are usually well correlated with the abundances of the involved elements. The depth of the C_2 lines depends for example mainly on the carbon excess. It increases if the [C−O] values listed in the legends of the panels become larger. However, for the strongest transitions the mentioned behaviour is less pronounced, since they are saturated, showing only weak variations due to the chemical mixture. In the warmer models with solar metallicity some of the C_2 lines also seem to be affected by an additional parameter possibly linked to [O/Z]. The intensity of the CN features increases when the values of [C−O], [N/Z], and [*Z*/H] grow. It should be noted that the combination of the last two quantities corresponds to the absolute nitrogen abundance. For the strong CN transitions we find only weak or no changes caused by different chemical mixtures, which is again connected to saturation. In some of these cases a higher [N/Z] results in slightly deeper lines. Finally, the intensity of the CO features increases for larger values of [O/Z] and [*Z*/H] where more oxygen is available.

A more complex relation between strength and elemental abundances can be found for blends containing at least two transitions of different species. The behaviour may change with effective temperature and metallicity, if these parameters influence the intensity ratio of the components. A good example is the feature at 1.70506 μm, which consists of a C_2 and a CO line. In the cooler models with [*Z*/H] = −1 the depth of this blend depends mainly on the carbon excess. We see a clear increase for larger [C−O] values, which has also been observed in the case of pure C_2 transitions. On the other hand, in the warmer COMARCS atmospheres having solar metallicity the behaviour resembles the one of a CO line, where the oxygen abundance is the dominant parameter. For the remaining two combinations of effective temperature and [*Z*/H] shown in Fig. 4 [C−O] and [O/Z] both play an important role.

Another interesting blend can be observed around 1.70548 μm. It comprises two lines produced by C_2 and by OH, which is a very rare species in the atmospheres of carbon stars. However, the appearance of such OH features shows that even in chemical equilibrium a small fraction of the oxygen is not bound in CO molecules. The corresponding excess will increase if the absolute abundance of the element grows due to a higher [O/Z] or [*Z*/H], and for lower [C−O] values. In the models having solar metallicity the intensity of the discussed blend changes according to these predictions. This means that the OH transition is the dominant component. For [*Z*/H] = −1 the behaviour becomes more complex, because the C_2 line, which gets stronger with a larger [C−O], plays a role.

3.4 Synthetic photometry

In the following text we discuss some typical examples for the photometric properties of the COMARCS atmospheres studied here. While in Fig. 5 ($J - K$) and ($H - K$) are shown as a function of the effective temperature, Fig. 6 contains a two-colour diagram ($J - H$) versus ($H - K$). All graphs cover the same sequences of models, which correspond to different abundance combinations. In Fig. 6 one can also find results from the previous carbon star grid by

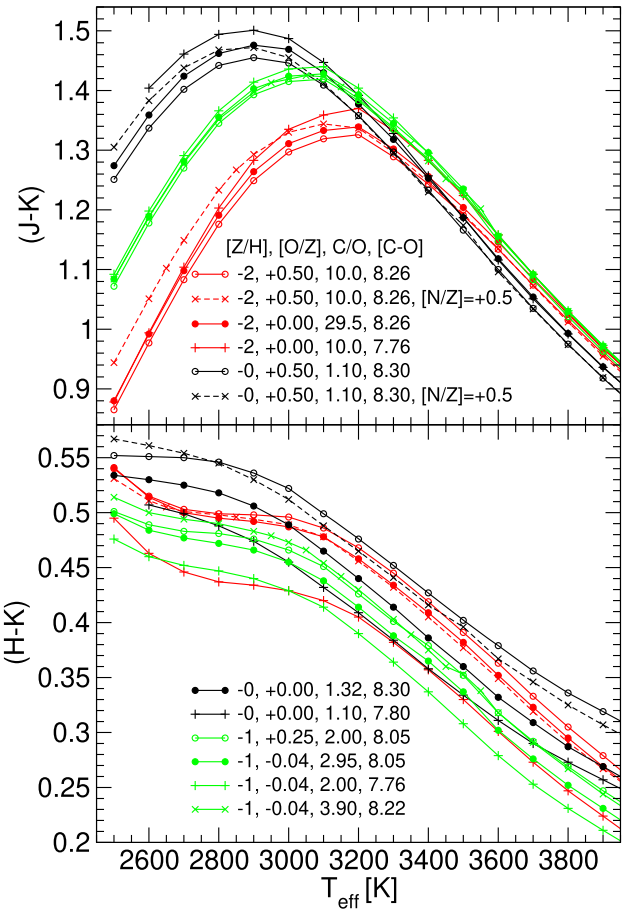

Figure 5. $(J - K)$ and $(H - K)$ as a function of the effective temperature for COMARCS models with $\log(g\ [\mathrm{cm\,s^{-2}}]) = 0.0$ and one solar mass. The colours correspond to different metallicities. For $[Z/H] = 0$ (black) and -2 (red) results obtained adopting $[O/Z] = +0.5$ (open circles) and $[O/Z] = +0.5$, $[N/Z] = +0.5$ (x, dashed lines) are compared to calculations for the standard composition ($[O/Z] = 0$, $[N/Z] = 0$) with a constant C/O (plus) or [C−O] (filled circles). In the case of $[Z/H] = -1$ (green) we show oxygen-enriched models having $[O/Z] = 0.25$, C/O = 2.0, and [C−O] = 8.05 (open circles) together with sequences where $[O/Z]$ is set to -0.04. They were created with the same C/O (plus), [C−O] (filled circles), and total amount of carbon ε_C (x).

Aringer et al. (2009) and observations. These data will be discussed in the following sections. For $[Z/H] = 0$ and -2 we compare COMARCS atmospheres with $[O/Z] = +0.5$ and $[O/Z] = +0.5$ plus $[N/Z] = +0.5$ to similar ones having a constant value of C/O or [C−O], where a scaled solar composition is assumed. In the case of $[Z/H] = -1$ the graphs include a sequence with an oxygen enrichment of $[O/Z] = +0.25$ at C/O = 2.0, which was taken from the stellar evolution calculations. It can be checked against models characterized by the primordial $[O/Z]$ of -0.04 and the same C/O, [C−O], or total amount of carbon.

In Fig. 5 one can see that the largest shifts in $(J - K)$ exceeding 0.1 mag appear below 3100 to 3200 K and are due to the different values for the overall metallicity. The stars get significantly bluer if $[Z/H]$ decreases. This effect is a lot stronger than the variations caused by a temperature offset of 100 K or by the deviations of individual abundances investigated here. The situation changes for the warmer models, where we find no clear trend with metallicity and the corresponding shifts become much smaller. In the range below 3000 to 3100 K an enrichment of nitrogen by $[N/Z] = +0.5$ gives a moderate reddening between about 0.03 and 0.06 mag, while it generates almost no differences or no differences if the stars are hotter. The COMARCS atmospheres having a constant C/O ratio in general get bluer when the amount of free carbon atoms [C−O] increases due to a higher $[O/Z]$. However, the corresponding shifts remain often very small, not exceeding 0.01 or 0.02 mag, for the shown examples. Only in the cooler models at solar metallicity and around 3000 to 3200 K at a lower $[Z/H]$ do we find moderate deviations, which grow in the case of $[O/Z] = +0.5$ up to about 0.05 or 0.06 mag. It should also be noted that the $(J - K)$ colours for the same [C−O] and different C/O are always quite similar, with offsets of less than 0.01 to 0.03 mag.

In the lower panel of Fig. 5 we observe also a strong influence of the metallicity on the $(H - K)$ colours of the COMARCS models. However, there is no clear trend and the corresponding differences are not larger than those caused by the studied variations of C/O or $[O/Z]$. The shifts produced by an enrichment of nitrogen remain in general quite small, never exceeding 0.02 mag for the shown cases with $[N/Z] = +0.5$. It is obvious that the amount of free carbon atoms plays an important role for the predicted $(H - K)$ colours. At all of the covered effective temperatures and metallicities they become redder if [C−O] increases. Adopting $[O/Z] = +0.5$ and a constant C/O ratio, the related offsets can get larger than 0.05 mag, corresponding to a model with identical abundances, which is much more than 100 K cooler. At least for the higher $[Z/H]$ values the amount of oxygen has some additional influence due to the CO lines. The colours turn bluer when the carbon excess remains the same and C/O increases. This effect is always weaker than the reddening caused by a larger [C−O], and it almost disappears for the lowest metallicities.

The appearance of the COMARCS atmospheres in the $(J - H)$ versus $(H - K)$ diagram presented in Fig. 6 reflects basically the temperature dependence shown in the two panels of Fig. 5, since $(J - H)$ and $(J - K)$ behave in a similar way. For both of the last-mentioned colours we find a clear trend that below 2800 to 3100 K cooler models again become bluer, which is much more pronounced in metal-poor stars. This reversion usually cannot be observed, because the corresponding objects are reddened by dust. The issue was already discussed in Aringer et al. (2009). All or almost all carbon stars with effective temperatures below 2800 to 3000 K have circumstellar shells generating significant shifts of the spectral energy distributions, which is also confirmed by the photometric measurements included in Fig. 6.

In Fig. 6 one can see that the deviations of the involved colours due to a higher nitrogen abundance of $[N/Z] = +0.5$ remain in general small compared to other effects. At the same time, we get considerable shifts if the value of [C−O] changes. For the shown examples these variations are always larger than the ones caused by a different C/O ratio at a constant carbon excess. Never the less, we find significant offsets also for the latter case when the metallicity becomes higher. The role of [C−O] and $[Z/H]$ as key parameters for the photometric properties will be discussed in the next section. Although those two quantities are very important for the spectra, their determination based on colours alone is usually not possible. The different dominating trends due to the abundances interact with each other, as one can see in Fig. 6, and with uncertainties concerning the effective temperatures, surface gravities, circumstellar reddening, and deviations from a hydrostatic structure.

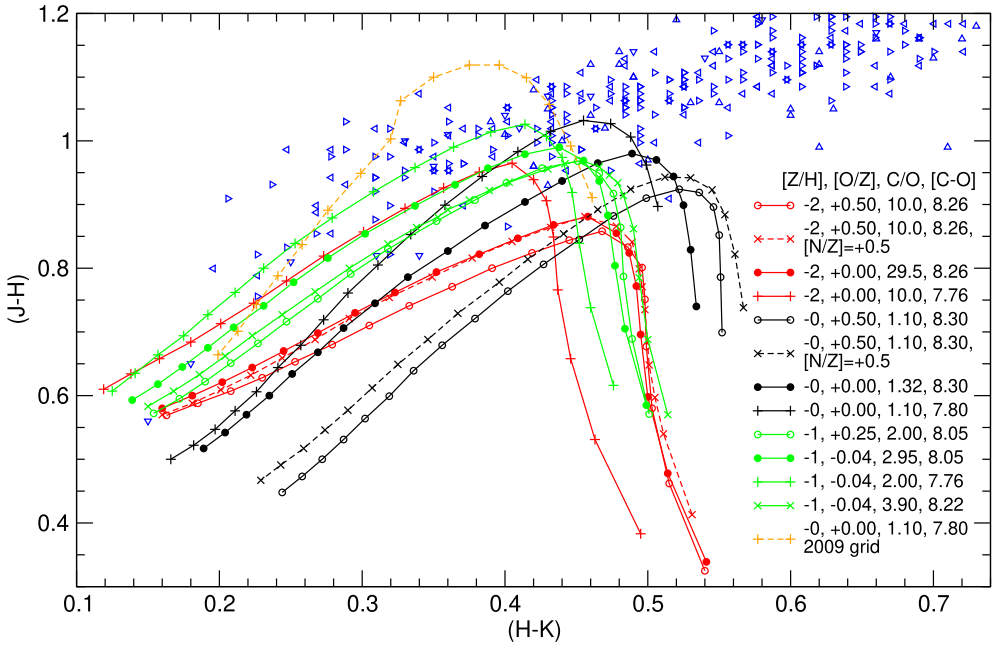

Figure 6. $(J - H)$ versus $(H - K)$ for temperature sequences of COMARCS models with $\log(g\ [\mathrm{cm\,s^{-2}}]) = 0.0$ and one solar mass. The shown abundance combinations and the corresponding colours and symbols are the same as in Fig. 5. In addition, we present results with $[Z/H] = 0.0$ and $C/O = 1.10$ taken from the previous COMARCS carbon star grid by Aringer et al. (2009), where the mass and surface gravity are identical (orange crosses, dashed line). The models are compared to observational data (blue triangles) listed in Bergeat, Knapik & Rutily (2001, up), Cohen et al. (1981, left), Costa & Frogel (1996, right), and Gonneau et al. (2016, down).

3.4.1 The carbon excess

One can conclude from the previous section that [C−O], which corresponds in principle to the amount of free carbon atoms not bound in CO, is an important parameter for the colours. In Figs 7–10 we show $(V - K)$, $(J - K)$, $(J - H)$, and $(H - K)$ as a function of this quantity. The plots cover all available abundance combinations listed in Table 1 and two effective temperatures. While 2800 K (upper panels) is typical for a cool carbon star, 3300 K (lower panels) represents a warmer one having only weak bands due to polyatomic molecules. The different colours in the graphs correspond to the included metallicities. Models with scaled solar standard mixtures (see Section 2.1.1) are shown as filled symbols connected by full lines. The positions of the various single characters representing the other abundance combinations indicate the expected deviations from these main relations when the amount of oxygen or nitrogen is changed for fixed values of [C−O] and [Z/H]. One can conclude for example that the slightly smaller primordial [O/Z] of −0.04 taken from the stellar evolution calculations (green crosses; see Section 2.1.3) causes almost no shifts. The plots also contain models from the previous carbon star grid by Aringer et al. (2009), which will be discussed in the following sections (orange dashed lines).

For the models with $[Z/H] = -1.0$ and an oxygen enrichment of $[O/Z] = 0.12$ or 0.25 taken from the stellar evolution calculations the deviations from the sequences of results obtained using scaled solar abundances always remain very small, if they are compared to the variations due to different values of the carbon excess. At 2800 K also the COMARCS atmospheres having $[O/Z] = 0.5$ and $[O/Z] = [N/Z] = 0.5$ are in most cases quite close to these standard relations. However, a few exceptions with moderate changes exist. Shifts of about 0.05 to 0.07 mag in $(J - K)$ and $(J - H)$ can be found for the lowest metallicity when the nitrogen abundance is increased. In addition, an oxygen enrichment at $[Z/H] = 0.0$ makes $(H - K)$ almost 0.03 mag redder. For 3300 K the relative deviations of models with $[O/Z] = 0.5$ and $[O/Z] = [N/Z] = 0.5$ often appear larger, which is at least partly due to the smaller variation of the colours as a function of the carbon excess. One should note that the upper and lower panels in the figures have different scales. The absolute offsets remain also for the warmer objects below about 0.03 to 0.06 mag. Compared to the consequences of changing the effective temperature, surface gravity, or optical depth of a possible dust shell this is not much.

The effect of using C/O (in the plot C/O − 1 for a better logarithmic representation) instead of [C−O] as a key parameter can be seen in Fig. 11, where we show $(J - K)$ as an example. In the corresponding two panels those COMARCS atmospheres, which have already been covered by the previous graphs featuring the carbon excess, are included keeping the same symbols, lines, and colours. When we compare the shifts caused by an oxygen abundance deviating from the scaled solar value to the ones in Fig. 8, it is obvious that they are always larger in the current diagram. Thus, using [C−O] and [Z/H] to characterize the chemical mixture gives more accurate predictions for $(J - K)$ than a similar combination involving the C/O ratio. The same is normally also true for most of the other colours.

4 DISCUSSION

In the following text we compare the photometric data obtained from the COMARCS models presented here to results based on the old (2009) carbon star grid. In addition, the impact of the current investigation on the predicted filter magnitudes for generating the observable properties of synthetic stellar populations will be discussed. Finally, we study the possibilities of measuring an enhancement of oxygen or nitrogen considering the behaviour of spectra and colours described in the previous sections as well as

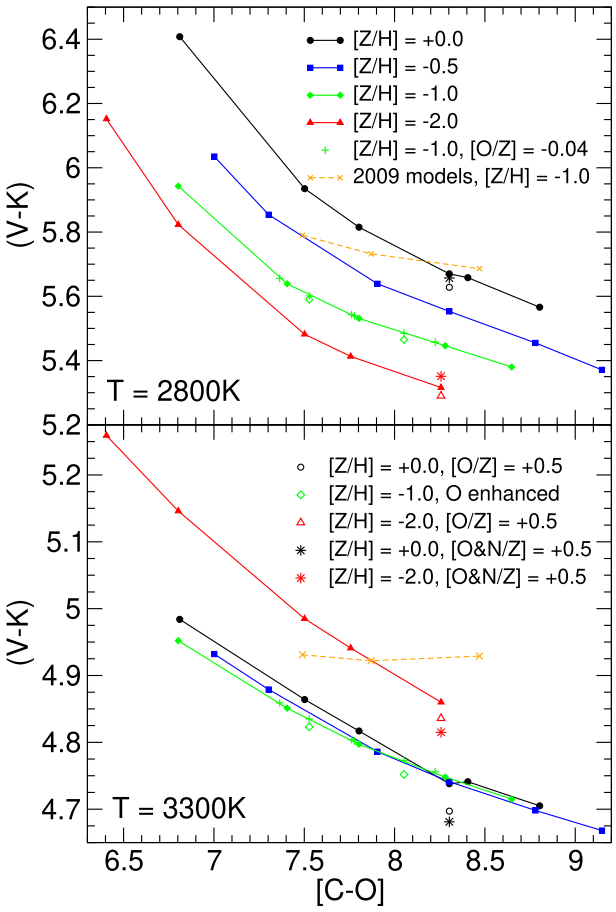

Figure 7. The $(V - K)$ colour as a function of [C−O] for COMARCS models with $\log(g\,[\mathrm{cm\,s^{-2}}]) = 0.0$ and one solar mass having $T_{\mathrm{eff}} = 2800$ K (upper panel) and 3300 K (lower panel). All abundance combinations used in this work and listed in Table 1 are included. The colours in the plot correspond to the different metallicities [Z/H]: 0.0 (black), −0.5 (blue), −1.0 (green), and −2.0 (red). Filled symbols connected by lines represent the sequences of models with standard composition where [O/Z] and [N/Z] remain 0.0. Green crosses mark results for [O/Z] = −0.04 at [Z/H] = −1.0. Open symbols stand for an enrichment of oxygen: [O/Z] = 0.5 at [Z/H] = 0.0 and −2.0, [O/Z] = 0.12 or 0.25 at [Z/H] = −1.0. An asterisk corresponds to an increased abundance of oxygen and nitrogen: [O/Z] = 0.5, [N/Z] = 0.5. We have also included models with [Z/H] = −1.0 and two solar masses (orange) taken from the previous COMARCS carbon star grid by Aringer et al. (2009).

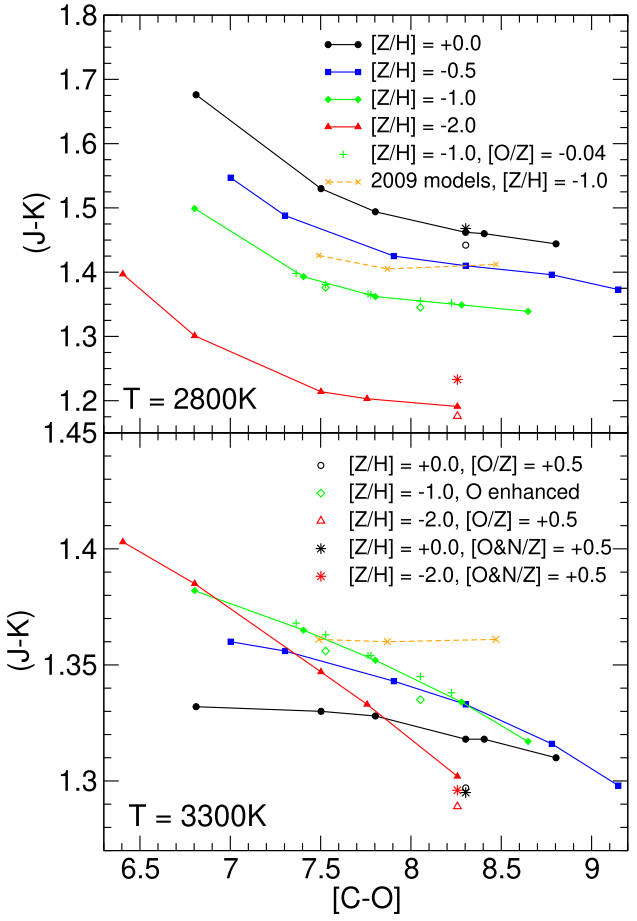

Figure 8. The $(J - K)$ colour as a function of [C−O]. The included COMARCS models and the corresponding symbols and line colours are the same as in Fig. 7.

uncertainties concerning temperatures, surface gravities, dynamical effects, and dust shells.

4.1 Comparison with the previous carbon star grid

In Figs 7−10, where colours are shown as a function of [C−O], we have also included a sequence of models with [Z/H] = −1.0 taken from the previous carbon star grid by Aringer et al. (2009). It should be noted that these results were calculated assuming 2.0 $M_\odot$, while all other COMARCS atmospheres used in our plots have 1.0 $M_\odot$. For the lower metallicities the old data base does not contain the corresponding objects with the smaller value. However, it has been demonstrated in Aringer et al. (2009) that changes of the mass at constant effective temperature and surface gravity cause only tiny colour shifts, which may in many cases be neglected. Also the slightly different abundances adopted for the solar mixture of the two grids will not generate significant deviations. Thus, we can conclude that the considerable offsets between old and new COMARCS models are mainly due to the updates concerning the molecular opacities described in Section 2. These variations often become larger than the shifts caused by a change of the metallicity or carbon excess.

As it was already shown by Aringer et al. (2009) the use of unscaled C_2 data, which became the standard for the new COMARCS models, results in a much better agreement of synthetic and observed $(H - K)$ or $(J - H)$ colours. This can be seen in Fig. 6, where we plot the two quantities against each other. The included sequence from the old grid with [Z/H] = 0.0, 1.0 $M_\odot$, and C/O = 1.10 remains for effective temperatures around 2900 to 3200 K outside the region covered by the measured values. For the corresponding new models having scaled solar abundances this is not the case. The situation could change if one assumes a considerable enrichment of oxygen. However, we do not expect that all observed carbon stars have [O/Z] values of about 0.3 or more, which may generate the necessary shifts. In the range above 3000 K there are also no significant deviations due to a different surface gravity, and objects with C/O ∼ 1.10 at solar metallicity should be common. Thus, we can confirm that the new COMARCS atmospheres allow a better reproduction of the measured colours. A detailed discussion concerning the observations is presented in Section 4.3.

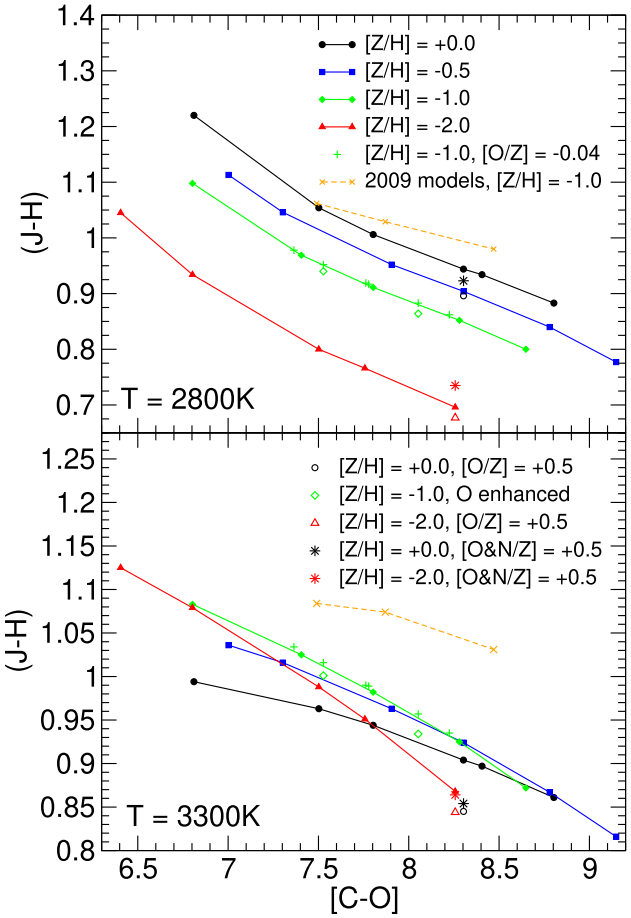

Figure 9. The $(J - H)$ colour as a function of [C−O]. The included COMARCS models and the corresponding symbols and line colours are the same as in Fig. 7.

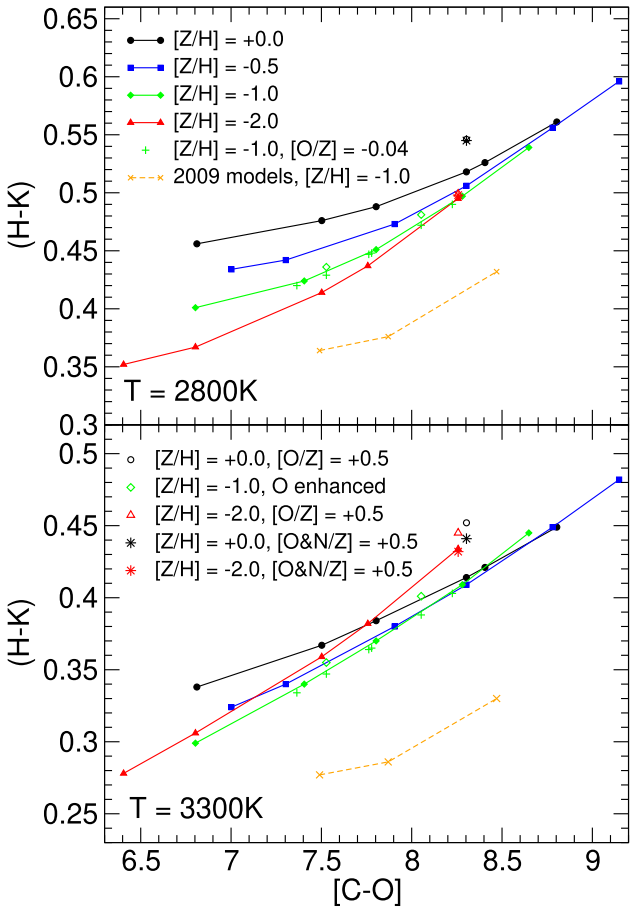

Figure 10. The $(H - K)$ colour as a function of [C−O]. The included COMARCS models and the corresponding symbols and line colours are the same as in Fig. 7.

In this context we also want to note that our preliminary tests with the new C_2 linelist from Yurchenko et al. (2018), which is considered to be more complete and accurate than the old one published by Querci et al. (1974), confirm our conclusion. The scaling used in the 2009 grid should not be applied, since it makes the predicted spectra worse. The data of Yurchenko et al. (2018) will become part of the standard opacity set-up for the next generation of COMA calculations.

4.2 Synthetic colours for stellar populations

In order to obtain absolute magnitudes or colours for isochrones and population synthesis from the photometric tables of the COMARCS grid, an interpolation in metallicity, effective temperature, surface gravity, and C/O ratio or [C−O] has to be performed. The stellar mass is treated as a correction factor, which may in the end be applied to the results. Our method was described in detail by Aringer et al. (2009). We use a linear interpolation taking [Z/H], $\log(g)$, and $\log(T_{\rm eff})$ for the first three parameters. An example for such calculations can be found in Marigo et al. (2017).

Since our systematic investigation of the effects caused by an increase of the oxygen and nitrogen abundances exists only for a limited sample of carbon star sequences with $\log(g\ [\mathrm{cm\,s^{-2}}]) = 0.0$ and one solar mass, an interpolation including the corresponding parameters [O/Z] and [N/Z] is not possible. The addition of two further dimensions would require a huge number of extra models, which simply takes too much time. Thus, [O/Z] and [N/Z] have to be considered as corrections applied to the results of the main computations. The corresponding values can be derived using the data produced for this work. Such a treatment is similar to the one of the stellar mass.

However, as it has been shown in Section 3.4.1, the deviations caused by increased abundances of oxygen and nitrogen are in most cases small if [Z/H] plus [C−O] remains constant and [O/Z] or [N/Z] does not exceed 0.5. The uncertainties due to effective temperatures, surface gravities, and reddening by dust will usually be larger. Thus, for the moment, we assume that it is not essential to introduce general corrections representing [O/Z] and [N/Z] when isochrones or similar data are calculated. Only for a stronger enrichment of oxygen and nitrogen with values above 0.5 can the colour changes become quite significant. Never the less, we do not expect that this happens very often in common carbon stars. In any case, it is important to use [C−O] instead of C/O, which, especially in cooler objects, keeps the possible errors small. A comparison of Figs 8 and 11 shows the consequences of adopting those two quantities as main parameters. It has already been said that with C/O the deviations are always bigger if one increases the abundance of oxygen. This is expected, since the absolute number of carbon atoms not bound in CO dominates the chemical equilibrium. A similar behaviour was found by Aringer et al. (2016) for very cool M giants, where [O−C] represents the important quantity.

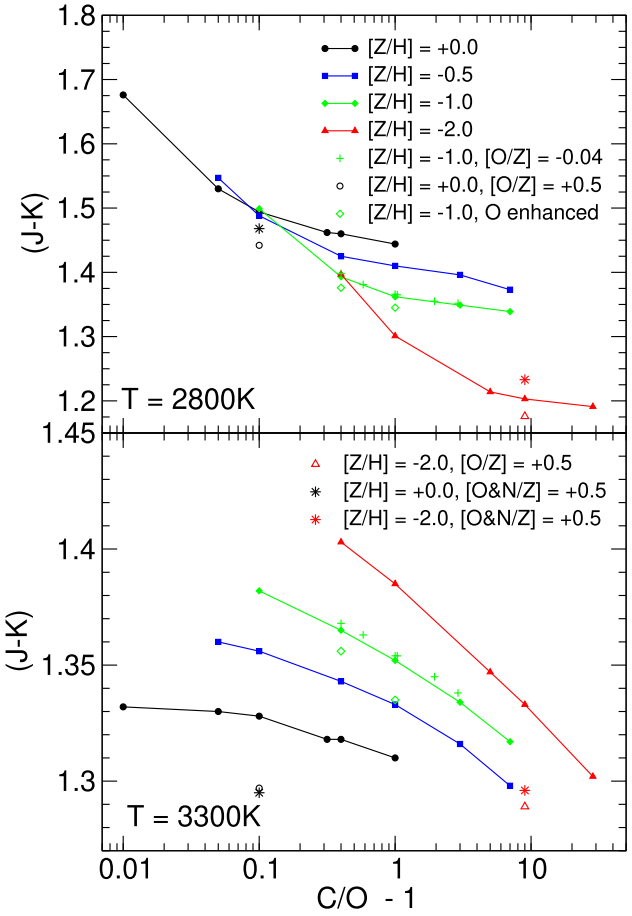

Figure 11. The $(J - K)$ colour as a function of C/O − 1. The included COMARCS models and the corresponding symbols and line colours are the same as in Fig. 7 except for the results from the previous carbon star grid, which are not shown here.

4.3 Models and observations

In this section we want to discuss to what extent photometric and spectroscopic observations can contribute to draw conclusions concerning carbon excess and oxygen or nitrogen enrichment.

4.3.1 Photometric observations

For the comparison of synthetic near-infrared colours based on the new COMARCS model grid against various observational data in Fig. 6 we adopted photometry from a few sources in the literature, which shall be described briefly in the following.

The first sample shown in the plot contains carbon stars in different parts of both Magellanic Clouds as well as in our Galaxy for which *J*, *H*, and *K* photometry was obtained by Cohen et al. (1981). From their tables 1−6 we could adopt for all of the sources values already corrected for interstellar reddening. An even more extended set of similar objects, namely C giants identified in the Large Magellanic Cloud, was later presented by Costa & Frogel (1996). The *J*, *H*, and *K* data from their table 3 are also dereddened and included in our plot. According to the latter authors, for both studies the same instrumental set-up was applied corresponding to the CIT/CTIO photometric system (Elias et al. 1982). The measurements were therefore converted to our standard colours following the equations given in table I of Bessell & Brett (1988).

In addition, the plot contains the collection of galactic C giants compiled from the literature by Bergeat et al. (2001) and used in Aringer et al. (2009). According to Knapik & Bergeat (1997) those observations can be directly compared to our synthetic photometry without any transformation. Finally, we show the colours derived from the spectra obtained by Gonneau et al. (2016) for carbon stars in the Magellanic Clouds and our Galaxy. Because of the different locations of the objects included in the plot, we expect that they cover a large metallicity range.

The most obvious thing in Fig. 6 is that the included hydrostatic models are able to explain the colours of the bluer carbon stars, while they fail completely to reproduce the observed objects with $(H - K) > 0.5$. As was already mentioned before, this behaviour is mostly caused by circumstellar reddening. Calculations simulating the effect of a dust shell around a COMARCS atmosphere can usually predict the photometric properties of the cooler C giants having mass-loss quite well (Srinivasan et al. 2011; Nanni et al. 2016, 2018).

The various covered values of metallicity, carbon excess, and oxygen enhancement produce considerable differences in the two-colour diagram, which have already been discussed in Section 3.4. We concluded there that it is difficult or impossible to obtain detailed information concerning the abundances from photometric indices alone, since the corresponding effects interact with each other and with uncertainties related to stellar parameters and circumstellar reddening. The situation might improve a bit if more and narrower filters are used. However, even from Fig. 6 one may deduce some basic results. For example, it is obvious that the warmest carbon stars with effective temperatures above 3600 K can only be described by models having a low metallicity. This conclusion will not change if we consider colour shifts due to a possible deviation of the surface gravities from our standard value. It agrees also with the fact that the corresponding objects are usually located in the Magellanic Clouds. In addition, for the warmer stars having no significant mass-loss the plot favours compositions where the carbon excess remains small, mostly not getting much larger than 8.0. On the other hand, in order to get winds driven by dust, higher [C−O] values are needed in the cooler giants, since enough material has to be available (Mattsson, Wahlin & Höfner 2010; Eriksson et al. 2014). Finally, we find no observed objects in the region where the models predict the location of the sources with solar metallicity and a strong enhancement of oxygen. Such carbon stars may still exist if they are obscured by a circumstellar shell.

4.3.2 Spectroscopic observations

Regarding the discussion of several selected low-resolution spectra in Section 3.2, it turns out that it will be very difficult or impossible to deduce quantities like [C−O], [O/*Z*], and [N/*Z*] from such data. Clear overall trends with the carbon excess or an enhancement of nitrogen appear if the fluxes are normalized relative to the continuum. However, due to the presence of many weak overlapping absorption lines this can never be measured in observed cool stars. In the unscaled spectra the effects of the abundance changes investigated here remain much less pronounced, which is at least partly caused by the strong influence of the molecular opacities on the atmospheric temperature–pressure structures. In addition, the relation between the intensity of certain features and the chemical composition may become complicated. For example, more nitrogen does not always result in deeper CN bands. This behaviour is also due to the saturation of stronger lines combined with a

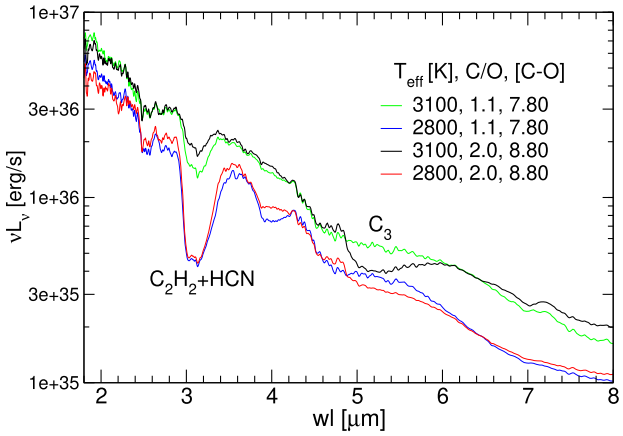

Figure 12. Low-resolution $R = 200$ infrared spectra computed from CO-MARCS models with $\log(g\ [\mathrm{cm\,s^{-2}}]) = 0.0$ and solar mass and metallicity. We show the effect of increasing C/O from 1.1 to 2.0 for $T_{\rm eff} = 2800$ and 3100 K. The standard composition with $[O/Z] = 0$ and $[N/Z] = 0$ is assumed. The strong features of C_2H_2 plus HCN at 3.2 μm and C_3 around 5 μm are marked.

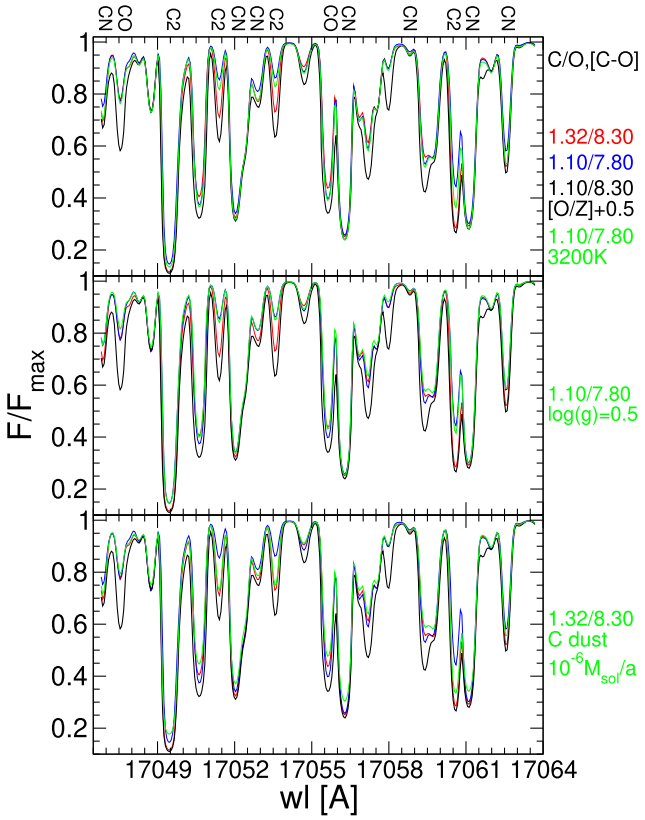

Figure 13. High-resolution $R = 300\,000$ spectra based on COMARCS models with $T_{\rm eff} = 3300$ K, $\log(g\ [\mathrm{cm\,s^{-2}}]) = 0.0$, and solar mass and metallicity having $[O/Z] = +0.5$ (black) and the standard composition ($[O/Z] = 0$) with a constant C/O = 1.10 (blue) or $[C-O] = 8.30$ (red). They are compared to calculations (green) for $[O/Z] = 0$ and C/O = 1.10, where $T_{\rm eff}$ was set to 3200 K (upper panel) or $\log(g\ [\mathrm{cm\,s^{-2}}])$ to +0.5 (central panel). In addition, we show results with $[O/Z] = 0$ and $[C-O] = 8.30$ that have been obtained assuming an outer carbon dust shell computed for a mass-loss rate of $10^{-6}\,M_\odot\,a^{-1}$ (green, lower panel). The data are normalized relative to their point with the largest flux. Absorption features produced by a single molecular species have been marked.

depression of the surrounding continuum by a large number of weak overlapping transitions, which are often at least partly produced by the same species. In connection with possible uncertainties concerning effective temperatures, surface gravities, reddening by circumstellar dust, and the flux calibration of the observations, the described conditions make it very difficult to obtain any information about abundances from low-resolution spectra of carbon stars.

A possible exception is the broad C_3 band around 5 μm, which could be used to determine [C−O], since the corresponding molecular abundance depends extremely on the amount of free carbon atoms (Jørgensen et al. 2000). In Fig. 12 we show for two effective temperatures (2800 and 3100 K) how its intensity increases with the C/O ratio. Also in this case a weakening of the feature due to saturation combined with a depression of the surrounding flux level appears if the stars become cooler than about 3000 K. The COMARCS atmosphere with C/O = 2.0 and 2800 K, which has by far the largest C_3 absorption in the plot, does not generate the most pronounced bump at 5 μm. In addition, the available hydrostatic and dynamic models do not manage to reproduce the depth and shape of the strongest C_3 bands correctly, which may be caused by a problem with the opacity data (independent of the chemical data discussed in Jørgensen et al. 2000).

For high-resolution spectra the situation is much better if one chooses a range where the quasi-continuous absorption of the weak molecular lines does not get too big. The data shown in Section 3.3 represent a good example. When saturated transitions and blends are excluded, we see a clear correlation between the intensity of features and the involved chemical abundances. This is an important condition for measuring the carbon excess and an enrichment of oxygen or nitrogen using lines of C_2, CN, HCN, CO, and other species. However, in order to evaluate the effect of a changed composition correctly, the treatment of molecular opacities for the generation of models and synthetic spectra has to be consistent.

In Fig. 13 we study the consequences of a possible dust shell and of uncertainties concerning the effective temperature or surface gravity. They are compared to some of the changes caused by abundance differences, which were discussed in Section 3.3. The plot includes three models shown already in Fig. 4 covering the same spectral range. For a star having $T_{\rm eff} = 3300$ K, $\log(g\ [\mathrm{cm\,s^{-2}}]) = 0.0$, and solar mass and metallicity we present a result with $[O/Z] = +0.5$ and two calculations, where the standard composition ($[O/Z] = 0$) is assumed keeping C/O = 1.10 or $[C-O] = 8.30$ constant. The variation due to the chemical mixture can then be compared to the consequences of decreasing $T_{\rm eff}$ by 100 K and increasing $\log(g\ [\mathrm{cm\,s^{-2}}])$ by 0.5. These are typical values of the uncertainties expected for the parameters of cool carbon stars. In order to be able to estimate the influence on the determination of abundances, we have marked all features that are produced by a single molecular species (no blend).

In the lower panel of Fig. 13 we show the effect of a dust shell consisting of amorphous carbon, which was computed using the spherical stationary wind code by Nanni et al. (2013, 2016) assuming a mass-loss rate of $10^{-6}\,M_\odot\,a^{-1}$. The corresponding opacity data were taken from Rouleau & Martin (1991). A COMARCS model with the same stellar parameters as all the others in the plot, $[O/Z] = 0$ and $[C-O] = 8.30$, has been adopted as the central radiation source. The higher carbon excess resulting in C/O = 1.32 was chosen for the comparison, since it favours the formation of dust. We assumed an initial outflow velocity of $4\,\mathrm{km\,s^{-1}}$, a

primordial grain size of 10^{-7} cm, and a normalized (relative to H) seed particle density of 1.058×10^{-12}. The contribution of the gas in the shell was neglected in the radiative transfer calculations carried out with the COMA code, which were also used to determine the temperatures of the solid material in the wind. We have adopted the chemical composition of the COMARCS model for all computations.

One can see that the studied changes of effective temperature and surface gravity have an impact on some of the absorption features. However, especially for the CO and C_2 lines, which are not saturated, the shown variations due to the abundances get much stronger. Thus, considering only the discussed uncertainties of the stellar parameters, it should be possible to measure differences of [C−O] or [O/Z] if they exceed values of about 0.2 to 0.3.

In our example also the attenuation of the absorption features caused by circumstellar dust, which affects mainly the stronger lines, is much weaker than some of the variations due to the abundances. Never the less, for higher mass-loss rates or [C−O] values and in other wavelength ranges the influence of such a shell could increase significantly. In extreme cases the spectral signature of the central atmosphere may disappear completely. The amount of dust present around an observed carbon star can usually be estimated from the overall energy distribution deduced from the combination of different photometric measurements (Srinivasan et al. 2011; Groenewegen 2012; Gullieuszik et al. 2012; Riebel et al. 2012; Nanni et al. 2018).

We conclude from our experiment that in stars with weak or moderate reddening due to circumstellar dust [$(J - K)$ up to about 3] the carbon excess and a possible enrichment of oxygen can be measured. The same applies to the nitrogen abundance, which may be determined using the CN lines. However, it was always assumed that the inner atmospheres behave like hydrostatic structures with radial symmetry. As we have already stated before, this approach will not work if the environment is dominated by pulsation, shock waves, and mass-loss. Such conditions appear mainly for the very cool carbon stars. In their dynamic atmospheres deviations from hydrostatic equilibrium and the related velocity fields change the intensities and profiles of lines, which may even result in emission components. Examples for the effect on high-resolution spectra of M and C giants can be found in Scholz (1992), Bessell, Scholz & Wood (1996), Winters et al. (2000), Nowotny, Höfner & Aringer (2010), Lebzelter et al. (2010), or Liljegren et al. (2017). It is obvious that for those objects an abundance determination will be difficult or impossible (McSaveney et al. 2007; Lebzelter et al. 2014).

Thus, the carbon excess and an enrichment of oxygen or nitrogen can only be measured in the atmospheres of giants when pulsation and mass-loss do not become too strong. On the AGB this corresponds usually to the less evolved and warmer stars. Additional uncertainties also affecting those objects may be due to deviations from spherical symmetry created by convection. For M supergiants the phenomenon and its consequences concerning high-resolution spectra were investigated by Chiavassa et al. (2011). In the case of extended carbon stars one might expect a similar behaviour. Finally, errors affecting line intensities and positions can cause further problems (Aringer 2005). First of all, this will have an impact on the identification of features produced by a single transition, since many of them are blends involving different species. A large part of the spectral signatures appears only in cool carbon stars, which prevents a calibration using warmer and less complicated atmospheres. However, the situation improves as better molecular line data become available (Tennyson & Yurchenko 2012; Barber et al. 2014; Brooke et al. 2014; Masseron et al. 2014; Sneden et al. 2014; Lyulin & Perevalov 2017; Chubb et al. 2018; Yurchenko et al. 2018). Unfortunately, not all of the new lists are complete in the temperature range important for the photospheres of red giants, which is a condition for their use in the calculation of model structures and broad stellar spectra.

5 CONCLUSIONS

In addition to our standard C star grid with scaled solar chemical mixtures, where only the amount of carbon has been increased, we have calculated sequences of hydrostatic COMARCS atmospheres assuming higher abundances of oxygen and nitrogen for a constant C/O, [C−O], or ε_C. This investigation remains restricted to models with $\log(g\ [\mathrm{cm\,s^{-2}}]) = 0.0$ and $1.0\,M_\odot$. Overall metallicities between $[Z/H] = 0.0$ and -2.0 are covered. The [C−O] values range from 6.41 to 9.15. The considered abundance changes may be caused by a combination of internal nuclear processes and convective mixing events appearing in evolved cool giants. They are expected following the predictions of stellar models and observations of post-AGB stars. Our study comprises [O/Z] and [N/Z] values up to $+0.5$.

Based on the atmospheric structures we have computed synthetic $R = 10\,000$ OS and convolved $R = 200$ low-resolution spectra as well as photometric data, which are all available at http://stev.oapd.inaf.it/atm.[2] The observable properties were derived using exactly the same set-up concerning opacities and abundances as in the models. Such a consistent treatment is important in order to obtain reliable results. For some of the COMARCS atmospheres we have also calculated high-resolution spectra allowing a study of individual lines.[3]

We find that it is difficult or not possible to get information about the abundances of oxygen and nitrogen as well as the carbon excess from our $R = 200$ spectra. When the lines are not resolved, changes of the visible continuum due to the influence of molecular opacities on the atmospheric structures and due to many weak overlapping transitions, plus saturation in regions with strong absorption, affect the appearance of the features. Their intensity may remain constant or show a complex behaviour if [O/Z], [N/Z], and [C−O] increase. This is combined with uncertainties concerning the flux calibration of the observations, the stellar parameters, or the impact of dust absorption, pulsation, and mass-loss. It has already been mentioned that the OS spectra, which have a higher resolution, cannot be compared directly to measurements.

For the high-resolution spectra we have demonstrated that it is in principle possible to measure an enrichment of oxygen plus nitrogen as well as the carbon excess if one chooses a region where at least some of the more intense CN, C_2, and CO lines are not blended or saturated and the influence of weak overlapping molecular transitions on the observed continuum remains limited. The changes produced by the typical uncertainties of the stellar parameters or a dust shell corresponding to a moderate mass-loss are in general smaller than the differences due to the abundance variations investigated here. However, as has been mentioned, when a star shows stronger pulsations and winds, any analysis based on

[2]Or also at http://starkey.astro.unipd.it/atm.

[3]Due to the discussed improvements we recommend that the users of our synthetic spectra and photometry for carbon stars should always take the data presented in this work and Aringer et al. (2016) instead of the old ones from Aringer et al. (2009) if new results are available for the selected parameters.

hydrostatic models will not work. In this case the optical depth of the envelope around the central object may become very large and dynamic processes like shocks or episodic outflow dominate the structures affecting line intensities and profiles. Such problems arise mainly for the coolest giants with $T_{\rm eff} < 3000$ K. Another possible source of errors is the molecular opacity data, which have an impact on the predicted strength of the measured features, the appearance of blends, and the influence of weak transitions on the continuum. The corresponding uncertainties also grow for lower temperatures. At high resolution it is again necessary to do the radiative transfer for the calculation of models and synthetic spectra in a consistent way.

For the photometric data circumstellar dust causes the strongest changes. Many of the observed carbon stars are in general much redder than all of the hydrostatic models. This affects again especially the coolest giants with $T_{\rm eff} < 3000$ K. Such objects can be described by adding a synthetic external shell to the central atmosphere or by a complete dynamic calculation including pulsation and mass-loss.

At a constant overall metallicity the carbon excess is the most important abundance parameter for the colours. We have shown that using [C−O] instead of C/O gives in general much better results if one neglects a possible deviation of the amount of oxygen from a scaled solar mixture. As has been mentioned, the COMARCS data base does not (and will not) cover variations of [O/*Z*] and [N/*Z*] with complete grids. However, like the stellar mass they may be included by correction terms derived from the existing model sequences and applied to the colours predicted for a certain combination of effective temperature, surface gravity, metallicity, and carbon excess. It is not possible to determine the corresponding abundances from photometric measurements alone, since problems similar to those discussed for the low-resolution spectra will appear. Never the less, even from the simple $(J-H)$ versus $(H-K)$ diagram shown in this work one can get some information. For example, it is obvious that the warmest carbon giants hotter than 3600 K are metal-poor. We may also exclude the frequent appearance of a strong enhancement of oxygen with [O/*Z*] around 0.5 in stars having a higher [*Z*/H] close to zero and a weak mass-loss.

In the future it could be useful to compute grids of dynamic models including pulsation, dust formation, and mass-loss with an enrichment of oxygen or nitrogen in order to cover also the cooler carbon giants. But even then it will remain very difficult to estimate the elemental abundances in these stars. We expect improvements concerning the hydrostatic atmospheres and synthetic spectra mainly from a lot of new molecular opacity data that are already available or may soon be available. The next versions of COMA and COMARCS will include them. Examples relevant for carbon stars are CN, CH, C_2, C_2H_2, and C_3.

ACKNOWLEDGEMENTS

This work was mainly supported by the European Research Council (ERC) Consolidator Grant funding scheme (*project STARKEY*, G.A. n. 615604). We thank Marco Dussin for helping us with the electronic publication of the data. AN acknowledges the support of the Centre National d'Études Spatiales (CNES). We thank Katy Chubb for her support concerning the text.

REFERENCES

Aringer B., 2000, PhD thesis, Univ. of Vienna, Univ. Wien
Aringer B., 2005, in Käufl H. U., Siebenmorgen R., Moorwood A., eds, Proceedings of an ESO Workshop, High Resolution Infrared Spectroscopy in Astronomy. ESO Astrophysics Symposia. Springer, Berlin, Heidelberg, p. 303
Aringer B., Jørgensen U. G., Langhoff S. R., 1997, A&A, 323, 202
Aringer B., Girardi L., Nowotny W., Marigo P., Lederer M. T., 2009, A&A, 503, 913
Aringer B., Girardi L., Nowotny W., Marigo P., Bressan A., 2016, MNRAS, 457, 3611
Barber R. J., Strange J. K., Hill C., Polyansky O. L., Mellau G. C., Yurchenko S. N., Tennyson J., 2014, MNRAS, 437, 1828
Bergeat J., Knapik A., Rutily B., 2001, A&A, 369, 178
Bessell M. S., 1990, PASP, 102, 1181
Bessell M. S., Brett J. M., 1988, PASP, 100, 1134
Bessell M. S., Scholz M., Wood P. R., 1996, A&A, 307, 481
Bladh S., Eriksson K., Marigo P., Liljegren S., Aringer B., 2019, A&A, 623, A119
Bressan A., Marigo P., Girardi L., Salasnich B., Dal Cero C., Rubele S., Nanni A., 2012, MNRAS, 427, 127
Brooke J. S. A., Ram R. S., Western C. M., Li G., Schwenke D. W., Bernath P. F., 2014, ApJS, 210, 23
Caffau E., Ludwig H.-G., Steffen M., 2009a, Mem. Soc. Astron. Italiana, 80, 643
Caffau E., Maiorca E., Bonifacio P., Faraggiana R., Steffen M., Ludwig H.-G., Kamp I., Busso M., 2009b, A&A, 498, 877
Chiavassa A., Freytag B., Masseron T., Plez B., 2011, A&A, 535, A22
Chubb K. L. et al., 2018, J. Quant. Spectrosc. Radiat. Transfer, 204, 42
Cohen J. G., Frogel J. A., Persson S. E., Elias J. H., 1981, ApJ, 249, 481
Costa E., Frogel J. A., 1996, AJ, 112, 2607
Dell'Agli F., Ventura P., Schneider R., Di Criscienzo M., García-Hernández D. A., Rossi C., Brocato E., 2015, MNRAS, 447, 2992
De Smedt K., Van Winckel H., Kamath D., Siess L., Goriely S., Karakas A. I., Manick R., 2016, A&A, 587, A6
Elias J. H., Frogel J. A., Matthews K., Neugebauer G., 1982, AJ, 87, 1029
Eriksson K., Nowotny W., Höfner S., Aringer B., Wachter A., 2014, A&A, 566, A95
Forestini M., Charbonnel C., 1997, A&AS, 123, 241
García-Hernández D. A., Ventura P., Delgado-Inglada G., Dell'Agli F., Di Criscienzo M., Yagüe A., 2016, MNRAS, 458, L118
Gonneau A. et al., 2016, A&A, 589, A36
Gonneau A. et al., 2017, A&A, 601, A141
Groenewegen M. A. T., 2012, A&A, 543, A36
Gullieuszik M. et al., 2012, A&A, 537, A105
Gustafsson B., Bell R. A., Eriksson K., Nordlund A., 1975, A&A, 42, 407
Gustafsson B., Edvardsson B., Eriksson K., Jørgensen U. G., Nordlund Å., Plez B., 2008, A&A, 486, 951
Herwig F., 2000, A&A, 360, 952
Herwig F., 2005, ARA&A, 43, 435
Höfner S., Bladh S., Aringer B., Ahuja R., 2016, A&A, 594, A108
Jørgensen U. G., Johnson H. R., Nordlund A., 1992, A&A, 261, 263
Jørgensen U. G., Hron J., Loidl R., 2000, A&A, 356, 253
Karakas A. I., Lattanzio J. C., 2014, PASA, 31, e030
Knapik A., Bergeat J., 1997, A&A, 321, 236
Lebzelter T., Nowotny W., Höfner S., Lederer M. T., Hinkle K. H., Aringer B., 2010, A&A, 517, A6
Lebzelter T., Nowotny W., Hinkle K. H., Höfner S., Aringer B., 2014, A&A, 567, A143
Liljegren S., Höfner S., Eriksson K., Nowotny W., 2017, A&A, 606, A6
Loidl R., Lançon A., Jørgensen U. G., 2001, A&A, 371, 1065
Lyulin O. M., Perevalov V. I., 2017, J. Quant. Spectrosc. Radiat. Transfer, 201, 94
Marigo P., Girardi L., Bressan A., Groenewegen M. A. T., Silva L., Granato G. L., 2008, A&A, 482, 883
Marigo P., Bressan A., Nanni A., Girardi L., Pumo M. L., 2013, MNRAS, 434, 488
Marigo P. et al., 2017, ApJ, 835, 77
Masseron T. et al., 2014, A&A, 571, A47
Mattsson L., Wahlin R., Höfner S., 2010, A&A, 509, A14
McSaveney J. A., Wood P. R., Scholz M., Lattanzio J. C., Hinkle K. H., 2007, MNRAS, 378, 1089

Nanni A., Bressan A., Marigo P., Girardi L., 2013, MNRAS, 434, 2390
Nanni A., Marigo P., Groenewegen M. A. T., Aringer B., Girardi L., Pastorelli G., Bressan A., Bladh S., 2016, MNRAS, 462, 1215
Nanni A., Marigo P., Girardi L., Rubele S., Bressan A., Groenewegen M. A. T., Pastorelli G., Aringer B., 2018, MNRAS, 473, 5492
Nowotny W., Höfner S., Aringer B., 2010, A&A, 514, A35
Nowotny W., Aringer B., Höfner S., Lederer M. T., 2011, A&A, 529, A129
Nowotny W., Aringer B., Höfner S., Eriksson K., 2013, A&A, 552, A20
Pastorelli G. et al., 2019, MNRAS, 485, 5666
Querci F., Querci M., Tsuji T., 1974, A&A, 31, 265
Riebel D., Srinivasan S., Sargent B., Meixner M., 2012, ApJ, 753, 71
Rouleau F., Martin P. G., 1991, ApJ, 377, 526
Scholz M., 1992, A&A, 253, 203
Sneden C., Lucatello S., Ram R. S., Brooke J. S. A., Bernath P., 2014, ApJS, 214, 26
Srinivasan S., Sargent B. A., Meixner M., 2011, A&A, 532, A54
Tennyson J., Yurchenko S. N., 2012, MNRAS, 425, 21
Werner K., Herwig F., 2006, PASP, 118, 183
Winters J. M., Keady J. J., Gauger A., Sada P. V., 2000, A&A, 359, 651
Yurchenko S. N., Szabó I., Pyatenko E., Tennyson J., 2018, MNRAS, 480, 3397

This paper has been typeset from a TEX/LATEX file prepared by the author.